inorganics

MDPI

Article

Effect of $[Zr(\alpha\text{-}PW_{11}O_{39})_2]^{10-}$ Polyoxometalate on the Self-Assembly of Surfactant Molecules in Water Studied by Fluorescence and DOSY NMR Spectroscopy

Thomas Quanten [1], Pavletta Shestakova [2], Aleksandar Kondinski [1] and Tatjana N. Parac-Vogt [1,*]

[1] Laboratory of Bioinorganic Chemistry, Department of Chemistry, KU Leuven Celestijnenlaan 200F, 3001 Leuven, Belgium; Thomas.quanten@gmail.com (T.Q.); aleksandar.kondinski@kuleuven.be (A.K.)

[2] Bulgarian NMR Centre, Institute of Organic Chemistry with Centre of Phytochemistry, Bulgarian Academy of Sciences, Acad. G. Bontchev Street, Bl.9, 1113 Sofia, Bulgaria; psd@orgchm.bas.bg

* Correspondence: tatjana.vogt@kuleuven.be; Tel.: +32-16-32-76-12

Received: 31 August 2018; Accepted: 8 October 2018; Published: 17 October 2018

Abstract: The catalytic fragmentation of hydrophobic proteins by polyoxometalates (POMs) requires the presence of surfactants in order to increase the solubility of the protein. Depending on the nature of the surfactant, different effects on the kinetics of protein hydrolysis are observed. As the molecular interactions between the POMs and surfactants in solutions have been scarcely explored, in this study, the interaction between the catalytically active Keggin polyoxometalate $[Zr(\alpha\text{-}PW_{11}O_{39})_2]^{10-}$ and four different surfactants—sodium dodecyl sulfate (SDS), dodecyldimethyl(3-sulfopropyl)ammonium (Zw3-12), dodecyldimethyl(3-sulfopropyl) ammonium (CHAPS), and polyethylene glycol *tert*-octylphenyl ether (TX-100)—have been studied in aqueous media. The effect of polyoxometalate on the self-assembly of surfactant molecules into micelles and on the critical micellar concentration (CMC) has been examined by fluorescence spectroscopy and diffusion ordered NMR spectroscopy (DOSY).

Keywords: polyoxometalates; zirconium; micelles; DOSY; surfactant; fluorescence; critical micellar concentration; micelle size

1. Introduction

Polyoxometalates (POMs) are anionic metaloxo clusters typically comprised of early transition metal centers in high oxidation states (mainly V, Mo, and W) [1]. POMs are well-known for their applications in the domains of catalysis [2,3] and molecular magnetism [4,5]. Over the past decade, our group has also explored the application of POMs as agents for the selective fragmentation of biomolecules [6–12].

The successful hydrolysis of proteins and other biological substrates is governed by a number of factors. One of the most important aspects is that both the protein substrate and the catalytic POMs are soluble in the same medium (i.e., water). In the case of the hydrolysis of hydrophobic proteins, a common approach to circumvent the low solubility (or often insolubility) of the proteins in aqueous solution is to use surfactants. However, as the surfactants exhibit polar or charged headgroups, they can also be involved in a variety of electrostatic or hydrogen bonding interactions with the POM [13]. This could hinder the binding of the POM to a protein, or it could inhibit their catalytic activity [14].

In order to address this issue, in this work, we seek to obtain molecular insights into the interactions between the $[Zr(\alpha\text{-}PW_{11}O_{39})_2]^{10-}$ polyoxoanion and commonly used

surfactants in biochemical applications, such as polyethylene glycol *tert*-octylphenyl ether (TX-100), dodecyldimethyl(3-sulfopropyl) ammonium (CHAPS), dodecyldimethyl(3-sulfopropyl)ammonium (Zw3-12), and surfactants—sodium dodecyl sulfate (SDS) (Figure 1), by using fluorescence spectroscopy and diffusion ordered NMR spectroscopy (DOSY). In the absence of POMs, water soluble surfactants at low concentrations populate the water/air interface. However, as the surfactant concentration gradually increases the interface becomes saturated and nanoscale supramolecular assemblies, such as micelles, are formed. The micelles form above a critical micellar concentration (CMC), which can be influenced by the following: (i) the charge of the hydrophilic headgroup, (ii) the length of the hydrophobic moiety, and (iii) the ionic strength of the solution [15]. Considering that POMs directly influence (i) and (iii), it is expected that the presence of POMs will influence the CMC. Furthermore, as POMs may be partially or fully encapsulated during the micelle formation, they may also affect the micellar size. The formation of surfactant encapsulated clusters (SECs) involving POMs is not unusual [16–18]. However, so far POM SECs have been mainly explored in non-aqueous media, although they have been attracting much attention in material science and catalysis [19,20].

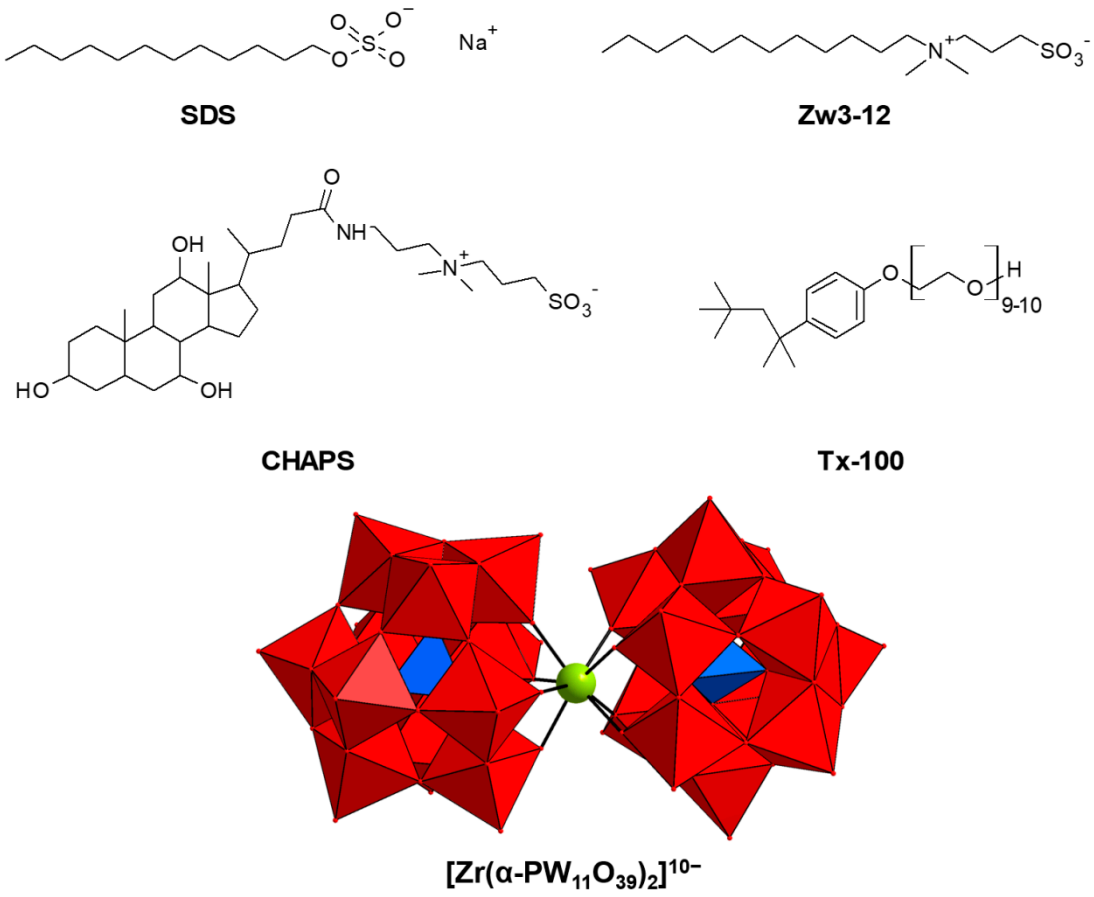

Figure 1. (**Top**) The molecular structures of the four studied surfactants: sodium dodecyl sulfate (SDS), dodecyldimethyl(3-sulfopropyl)ammonium (Zw3-12), 3-[(3-cholamidopropyl)dimethylammonio]-1-propanesulfonate (CHAPS), polyethylene glycol *tert*-octylphenyl ether (TX-100). (**Bottom**) Combined polyhedral and ball-and-stick representation of $[Zr(\alpha\text{-}PW_{11}O_{39})_2]^{10-}$ (**1**). Color code: WO_6—red octahedral; PO_4—blue tetrahedral; and Zr^{IV}—green spheres.

In this work, we first explore the effect of **1** on the CMC using fluorescence spectroscopy, which is then followed by detailed ^1H and ^{31}P DOSY studies [21–23]. The POM, $[Zr(\alpha\text{-}PW_{11}O_{39})_2]^{10-}$ (**1**), is used as the salt, $(Et_2NH_2)_{10}[Zr(\alpha\text{-}PW_{11}O_{39})_2]$ throughout the study. This POM has previously been shown to exhibit catalytic activity towards the hydrolysis of different proteins [13,14].

2. Results and Discussion

2.1. The Interaction between Micelles and ***1*** *Studied Using the Pyrene Fluorescence Method*

In 1977, Kalyanasundaram and Thomas demonstrated that the fluorescence intensity of the vibronic fine structure of the pyrene monomer fluorescence is strongly solvent dependent [24]. Pyrene is characterized by five distinct vibronic peaks at 372 nm, 378 nm, 383 nm, 389 nm, and 392 nm, which are labeled I, II, III, IV, and V, respectively. The ratio of the vibronic peaks at 372 nm and 383 nm (typically referred to as the I:III pyrene ratio) is indicative of a micelle formation and has become a popular method for the determination of the CMC of surfactant solutions [25]. At surfactant concentrations below the CMC, the I:III ratio corresponds to a polar environment. When the surfactant concentration increases, the ratio decreases rapidly as the pyrene molecules sense the hydrophobic environment of the interior of the micelle. Above the CMC, the I:III ratio remains roughly constant when pyrene is incorporated into the micelle.

This method has been widely used to study surfactants [26–29], mixed-surfactant systems [30,31], block-*co*-polymers [32–34], and the additive and temperature effects on the micellar properties of surfactants [35,36]. The emission spectrum of a saturated aqueous solution of pyrene at pH 7.4 (10 mM sodium phosphate buffer) is shown in Figure 2 and Figure S1a.

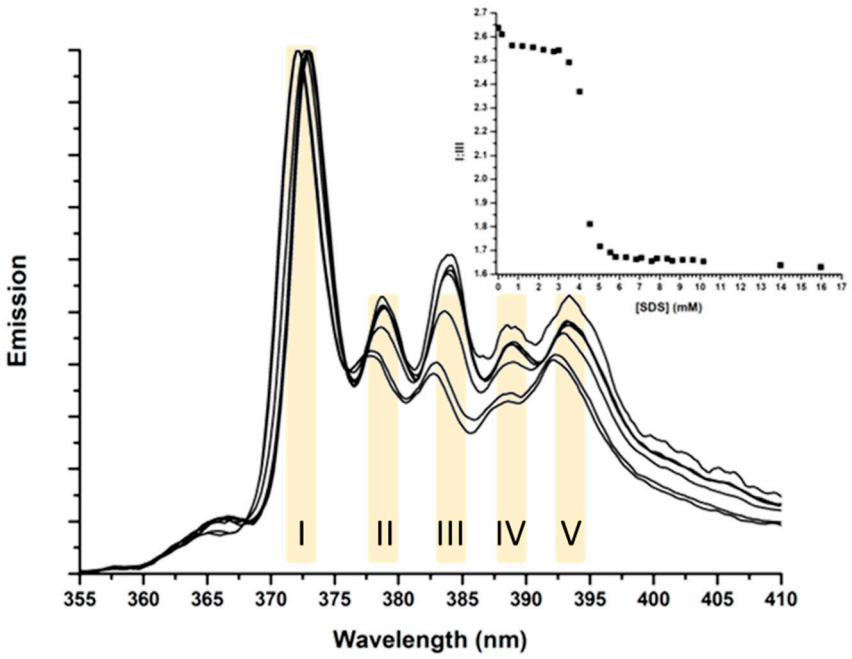

Figure 2. The emission spectra of the normalized emission of a saturated pyrene solution (2–3 μM) buffered at pH 7.4 by a 10 mM sodium phosphate solution, in the presence of increasing concentrations of SDS. (**Inset**) The intensity ratios of peak I to peak III plotted in the function of the SDS concentration in mM.

The ratio of the fluorescence intensity of peak I to III plotted in the function of the surfactant concentration follows a Boltzman-type sigmoidal decrease (see inset Figure 2), which can be fitted to Equation (1).

$$\mathrm{I:III} = \frac{A_1 - A_2}{1 + \exp((x - x_0)/\Delta x)} + A_2 \quad (1)$$

Where I:III stands for the intensity ratio of peak I to III; x stands for the surfactant concentration, A_1 and A_2 are the upper and lower limits of the sigmoid, respectively; x_0 is the center of the sigmoid; and Δx is related to the surfactant concentration range wherein the abrupt decrease of I:III occurs.

According to Aguiar et al., the CMC of a surfactant is determined according to Equation (2) or Equation (3) [37], as follows:

$$CMC_1 = x_0, \text{ if } x_0/\Delta x \geq 10 \quad (2)$$

$$CMC_1 = x_0 + 2 \times \Delta x, \text{ if } x_0/\Delta x < 10 \quad (3)$$

Generally, Equation (2) is used for surfactants with a high CMC, while Equation (3) is employed for low CMC values, typically below 1 mM. This different criterion has been explained in terms of the pyrene partition between the micelles and bulk solution. When the volume of the hydrophobic phase is not sufficient, pyrene is divided between the micelles and the bulk water, thereby providing an average I:III value that corresponds to a more polar environment, consequently prolonging the transition from high to low I:III ratios [38]. The calculated CMC values are summarized in Table 1 according to Equation (2) or Equation (3).

Table 1. The calculated critical micellar concentration (CMC) values (in mM) of the different surfactants in the environments listed in the first column.

	SDS	TX-100	CHAPS	Zw3-12
[a, b]	4.16 ± 0.01	0.41 ± 0.08	5.80 ± 0.1	2.28 ± 0.03
16 mM Et_2NH_2Cl [a]	1.44 ± 0.01	0.26 ± 0.04	5.55 ± 0.05	2.30 ± 0.03
1% **1** [a]	1.40 ± 0.01	0.23 ± 0.05	2.0 ± 0.4	1.10 ± 0.05 [c]

[a] All of the samples were buffered at pH 7.4 by a 10 mM sodium phosphate buffer; [b] Without **1** or its counterion ($Et_2NH_2^+$) present; [c] CMC was calculated from the I:II ratio instead of the I:III because of the overlap of peak II and III. SDS—sodium dodecyl sulfate; TX-100—polyethylene glycol *tert*-octylphenyl ether; CHAPS—dodecyldimethyl(3-sulfopropyl) ammonium; Zw3-12—dodecyldimethyl(3-sulfopropyl)ammonium; **1**—$[Zr(\alpha\text{-}PW_{11}O_{39})_2]^{10-}$.

The CMC of the SDS in pure water is reported to be 8 mM [37]. In a 10 mM sodium phosphate buffer at pH 7.4, the CMC is reduced to 4.16 mM. This decreases further to 1.40 mM in the presence of 1% **1**. However, in the presence of 16 mM Et_2NH_2Cl, which is the approximate concentration of counterions that accompany 1% of **1** in a solution, the same CMC was observed. This indicates that the $Et_2NH_2^+$ cation is responsible for lowering the CMC of SDS, probably because of the screening of the repulsive anionic–anionic interactions, and not the POM polyanion itself. The CMC of TX-100 was increased from the reported 0.15–0.23 mM to 0.41 mM at pH 7.4 [39–43]. In the presence of $Et_2NH_2^+$, the CMC was reduced to 0.26 mM, which was similar to the CMC in the presence of 1% of **1** (0.23 mM), again demonstrating that the POM itself has no significant influence on the CMC of TX-100. The CMC values that were determined at pH 7.4 for CHAPS and Zw3-12 (5.8 and 2.28 mM, respectively) fall within the range of the reported values for CHAPS (3 to 11 mM) [43–48] and Zw3-12 (2 to 4 mM) [49–51]. Both of the surfactants were unaffected by the presence of Et_2NH_2Cl, but in the presence of 1% **1**, the CMC decreased to 2.0 mM and 1.10 mM for CHAPS and Zw3-12, respectively. This indicates that **1** screens the repulsive forces between the zwitterionic groups, allowing them to form micelles more easily.

The structural information of the micelles can be derived from the I:III pyrene ratio as it is sensitive to its local environment. When the hydrophobicity of the local environment increases, the I:III ratio decreases. If additional water molecules permeate the micelle surface, then the ratio increases. Hence, the ratio can be used as a measure for the compactness of the head group packing at the micelle surface [24,25]. The I:III ratios of the pyrene populating the interior of the micelles in different conditions are summarized in Table 2.

The I:III ratio of pyrene dissolved within an SDS micelle is unaffected by the addition of Et_2NH_2Cl or **1**, indicating that the packing of the polar, charged head groups remains the same. The surface of a TX-100 micelle becomes more compact when 1% of the POM is added, despite the unaffected CMC value. It is known that POMs can bind with polyether functions, and a similar binding could explain the closer packing of the polyethylene glycol head groups of TX-100. The I:III ratio of CHAPS was

relatively unaffected by the addition of Et_2NH_2Cl, but in the presence of **1**, the ratio decreased slightly. The POM probably shields the repulsive forces between the ammonium groups, but the vicinity of the anionic sulfonate causes repulsive interactions, avoiding a close packing of the head groups. Unfortunately, because of the overlapping peaks of the pyrene emission spectrum in the presence of Zw3-12, a I:III ratio could not be determined for these micelles (see Figure S1b in Supplementary Materials). However, because of the similar trend in the CMC values of Zw3-12 and CHAPS, one can assume that a similar trend would be observed for the packing of the micelle surface of Zw3-12.

Table 2. The intensity ratio I:III [a] of the vibronic peaks I to III of pyrene within the micelles.

	SDS	TX-100	CHAPS	Zw3-12
[b, c]	1.66 ± 0.01	1.97 ± 0.01	1.24 ± 0.02	2.03 ± 0.01
16 mM Et_2NH_2Cl [b]	1.67 ± 0.01	2.00 ± 0.01	1.28 ± 0.01	2.01 ± 0.01
1% **1** [b]	1.64 ± 0.01	1.83 ± 0.01	1.17 ± 0.02	[d]

[a] The lower limit (A_2) of the Boltzman sigmoidal fit (see Equation (1)) was taken as the I:III ratio of pyrene populating the interior of the micelle; [b] All of the samples were buffered at pH 7.4 by a 10 mM sodium phosphate buffer; [c] Without **1** or its counterion ($Et_2NH_2^+$) present; [d] No I:III ratio could be calculated because of the overlap of peak II and III.

2.2. The Interaction between Micelles and *1* Studied by DOSY

DOSY is a 2D NMR technique that spectroscopically differentiates between particles in solution based on their translational self-diffusion coefficient (D). A DOSY spectrum consists of a standard 1D spectrum on the F2 (horizontal) axis and the diffusion coefficients in the F1 (vertical) dimension (see Figure 3 and Supplementary Materials), thus correlating the chemical shifts with the diffusion coefficients of the different components present in the solution.

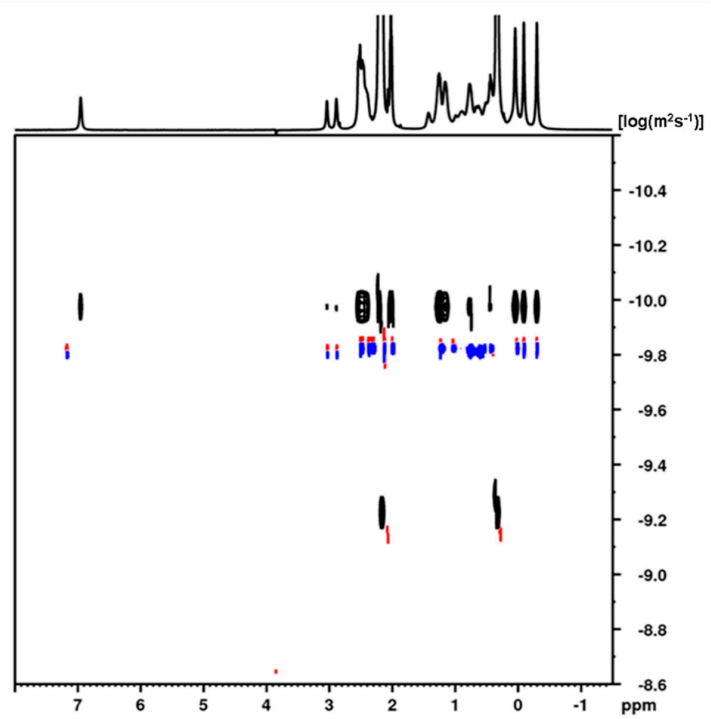

Figure 3. The ^1H diffusion ordered NMR spectroscopy (DOSY) spectra of 50 mM of CHAPS in the absence of **1** and Et_2NH_2Cl (blue) and in the presence of 90 mM Et_2NH_2Cl (red) and 9 mM **1** (black) at pH 7.4 (10 mM sodium phosphate buffer) and 20 °C.

The diffusion dimension in the DOSY spectra is normally given in a logarithmic scale (as log D values in [log($m^2 \cdot s^{-1}$)] units), which is a more convenient presentation when there is a large difference in the diffusion coefficients of the different components of the studied mixture.

The diffusion coefficient of a compound is determined by its size, weight, and shape. If the compounds interact, their diffusion coefficient will decrease because of the larger size and molecular weight of the formed complex [52].The diffusion coefficients of the different surfactants, the counter ion ($Et_2NH_2^+$), and the POM cluster measured in their individual solutions and in the mixtures with a given composition are summarized in Table 3.

Table 3. The translational self-diffusion coefficients (D) of the surfactants in the presence or absence of **1** and the counterion ($Et_2NH_2^+$) (measured with ^{1}H DOSY); and of **1** in the absence or presence of the different surfactants (measured with ^{31}P DOSY). The concentrations of the surfactants and **1** are 50 mM and 9 mM, respectively.

Sample	Compound	D × 10^{-11} ($m^2 \cdot s^{-1}$)
Et_2NH_2Cl [a]	$Et_2NH_2^+$	70.5
$Et_2NH_2^+$ + 1 [b]	$Et_2NH_2^+$ **1**	51.1 20.9 [d]
CHAPS	CHAPS	14.5
CHAPS + 9 mM 1	CHAPS $Et_2NH_2^+$ **1**	8.78 43.2 8.21 [d]
CHAPS + Et_2NH_2Cl [c]	CHAPS $Et_2NH_2^+$	14.1 63.9
Zw3-12	Zw3-12	11.5
Zw3-12 + 9 mM 1	Zw3-12 $Et_2NH_2^+$ **1**	6.12 40.4 9.24 [d]
Zw3-12 + Et_2NH_2Cl [c]	Zw3-12 $Et_2NH_2^+$	10.8 65.8
TX-100	TX-100	4.55
TX-100 + 9 mM 1	TX-100 $Et_2NH_2^+$ **1**	4.46 45.9 16.9 [d]
TX-100 + Et_2NH_2Cl [c] **SDS**	TX-100 $Et_2NH_2^+$ SDS	4.63 65.6 9.49
SDS + 9 mM 1	SDS $Et_2NH_2^+$ **1**	6.76 39.9 19.5 [d]
SDS + Et_2NH_2Cl [c]	SDS $Et_2NH_2^+$	8.22 26.0

[a] 90 mM Et_2NH_2Cl; [b] 9 mM of **1**; [c] 90 mM of Et_2NH_2Cl was added; [d] Determined from ^{31}P diffusion ordered NMR spectroscopy (^{31}P DOSY).

With the aim to independently asses the interaction of the surfactant with the counterion $Et_2NH_2^+$ and with the POM polyanion, we first measured a DOSY spectrum of a mixture of each surfactant and Et_2NH_2Cl.

The results demonstrate that the interaction between the CHAPS micelles and $Et_2NH_2^+$ is negligible, as only a minor decrease in their diffusion coefficients was detected (see Table 3). The slight decrease of the D value of $Et_2NH_2^+$ from 70.5 × 10^{-11} $m^2 \cdot s^{-1}$ in its neat solution to 63.9 × 10^{-11} $m^2 \cdot s^{-1}$ in the mixture with CHAPS indicates that the counterion is likely to be involved in a fast equilibrium between its free

state and its micelle bound state, which is strongly shifted toward the free state. These observations are in agreement with the pyrene fluorescence studies showing that the presence of the $Et_2NH_2^+$ counterion resulted in a minor decrease of the CMC of CHAPS (Table 1). In the following step, the mixture of CHAPS and **1** was investigated. Figure 3 shows the DOSY spectrum of a mixture of 50 mM CHAPS in the absence and in the presence of 9 mM of **1** or 90 mM of Et_2NH_2Cl. The spectrum demonstrates that in the surfactant/POM mixture, the diffusion coefficient of CHAPS (8.78×10^{-11} $m^2 \cdot s^{-1}$) is much lower (by a factor of 1.7) compared with the value measured in both the individual CHAPS solution and in the CHAPS/Et_2NH_2Cl mixture (Table 3). The same effect was observed by ^{31}P DOSY for the diffusion coefficient of the POM cluster, which was 2.6 times lower in the mixture. The relatively close values of the diffusion coefficients of the CHAPS (8.78×10^{-11} $m^2 \cdot s^{-1}$) and **1** (8.21×10^{-11} $m^2 \cdot s^{-1}$) suggest the formation of a relatively stable micelle/POM complex because of the electrostatic interactions between the negatively charged POM and the positively charged quaternary ammonium group of CHAPS. The diffusion coefficient of the counterion $Et_2NH_2^+$ in the CHAPS/**1** mixture (43.2×10^{-11} $m^2 \cdot s^{-1}$) was lower by a factor of 1.2 and 1.5, respectively, compared with its value in the individual solution of **1** (51.1×10^{-11} $m^2 \cdot s^{-1}$) and in the CHAPS/Et_2NH_2Cl solution. This trend could be explained by the weak binding of the counterion to the larger CHAPS/POM complex, probably through its interaction with the negatively charged POM and, to a lesser extent, with the sulfonate group of the CHAPS. This proposal is corroborated by the higher D value of the counterion measured in the CHAPS/Et_2NH_2Cl solution (63.9×10^{-11} $m^2 \cdot s^{-1}$), compared with its diffusion coefficient in the individual solution of **1** (51.1×10^{-11} $m^2 \cdot s^{-1}$), showing that the counterions interact more strongly with the POM cluster than with the negatively charged sulfonate groups of the surfactant micelles. The higher diffusion coefficient of the counterion compared with the diffusion coefficients of both the surfactant and the POM indicates that it is involved in a dynamic equilibrium between the bulk solution and the CHAPS/POM/$Et_2NH_2^+$ complex.

A similar trend was observed for the diffusion coefficients of the other zwitterionic surfactant Zw3-12, the counterion $Et_2NH_2^+$, and the POM cluster in both the Zw3-12/Et_2NH_2Cl and Zw3-12/**1** mixtures (Table 3 and Figures S1–S3). In the Zw3-12/**1** mixture, the diffusion coefficients of the Zw3-12 and the counterion $Et_2NH_2^+$ were significantly lower compared with their values measured in the Zw3-12/Et_2NH_2Cl solution, indicating the formation of the Zw3-12/**1**/$Et_2NH_2^+$ complex. However, the diffusion coefficient of the POM cluster (9.24×10^{-11} $m^2 \cdot s^{-1}$) measured by ^{31}P DOSY in the Zw3-12/**1** mixture was larger than the D value of the surfactant (6.12×10^{-11} $m^2 \cdot s^{-1}$). The 1D ^{31}P spectrum of the Zw3-12**/1** mixture shows only one signal at −14.69 ppm, contrary to the ^{31}P spectrum of pure **1**, which displays two resonances at −14.57 and −14.65 ppm, which is characteristic of the dimeric mono-Zr substituted Keggin POM because of the presence of two units with different bonding modes (bond lengths and bond angles), as determined by X-ray crystallography [53,54]. The observed changes in the ^{31}P spectrum indicate that in the presence of Zw3-12 micelles, **1** undergoes structural transformations towards a monomeric kegginoidal polyoxoanion [53–55], with a lower overall negative charge than the parent dimeric $[Zr(\alpha\text{-}PW_{11}O_{39})_2]^{10-}$ cluster. A probable cause of this is the weaker electrostatic interactions between the positively charged ammonium group of the Zw3-12 and the POM cluster. The lower stability of the Zw3-12/POM complex corroborates the observed differences in the micellar and POM diffusion coefficients, as in this scenario, the contribution of the free micelles and that of the free POM species to the measured diffusion coefficients are expected to be more pronounced. These results indicate that the POM/micelle/$Et_2NH_2^+$ complex formed in the Zw3-12/**1** solution is different from the complex in CHAPS/**1** mixture (see above), which also corroborates the differences in the pyrene spectra (see Figure S1b).

The minor decrease in the diffusion coefficient of the SDS/**1** mixture measured by the ^{31}P DOSY (from 20.9×10^{-11} $m^2 \cdot s^{-1}$ in its pure solution to 19.5×10^{-11} $m^2 \cdot s^{-1}$ in the SDS/**1** mixture) corroborates that the anionic SDS micelles do not interact with **1**. However, the diffusion coefficient of the SDS micelles decrease from 9.49×10^{-11} $m^2 \cdot s^{-1}$ in the pure SDS solution to 6.76×10^{-11} $m^2 \cdot s^{-1}$ in the presence of 9 mM **1**, because of the interaction of the negatively charged sulfate group of the

surfactant with the cationic $Et_2NH_2^+$ counterion of the POM. This interaction is further confirmed by the observed decrease in the diffusion coefficients of both the surfactant and the $Et_2NH_2^+$ counterion in the SDS/Et_2NH_2Cl mixture (Table 3). The higher diffusion coefficient of $Et_2NH_2^+$ measured in the SDS/**1** mixture (39.9×10^{-11} $m^2 \cdot s^{-1}$) compared with its value in the SDS/Et_2NH_2Cl mixture (26.6×10^{-11} $m^2 \cdot s^{-1}$) suggests that in the SDS/**1** mixture, the counterion is most probably involved in a complex dynamic equilibrium because of its competitive interactions with both the SDS micelles and the polyoxoanion.

The final surfactant, the neutral TX-100 ($D_{pure} = 4.55 \times 10^{-11}$ $m^2 \cdot s^{-1}$), was largely unaffected by the presence of **1** ($D_{\mathbf{1}} = 4.46 \times 10^{-11}$ $m^2 \cdot s^{-1}$) or Et_2NH_2Cl ($D_{count} = 46.3 \times 10^{-11}$ $m^2 \cdot s^{-1}$), as only minor changes of its diffusion coefficient were detected in both the TX100/**1** and TX100/Et_2NH_2Cl mixtures. As expected, because of the lack of any charge, TX-100 does not actually interact with **1** or the counter ion.

3. Materials and Methods

Deuteriumoxide (D_2O), phosphotungstic acid hydrate ($H_3[PW_{12}O_{40}] \cdot xH_2O$), disodium phosphate ($Na_2HPO_4$), sodium dodecyl sulfate (SDS), pyrene, CHAPS, and Zw3-12 were purchased from Sigma-Aldrich BVBA (Overijse, Belgium). The zirconium oxychloride octahydrate was purchased from Chem-Lab Analytical BVBA (Zedelgem, Belgium). The aqueous hydrochloric acid (37%) and potassium hydrogen carbonate were obtained from Acros Organics BVBA (Geel, Belgium). The ethanol, sodium hydrogen carbonate, aqueous *ortho*-phosphoric acid (85%), and diethyalaminehydrochloride were purchased from Thermo Fisher Scientific BVBA (Geel, Belgium). The methanol and monosodiumphosphate (NaH_2PO_4) and the potasium chloride were purchased from VWR International BVBA (Leuven, Belgium). The $(Et_2NH_2)_{10}[Zr(\alpha\text{-}PW_{11}O_{39})_2]$ (**1**) was synthesized following the previously reported procedures [53,54].

Emission spectroscopy: All of the samples were buffered at pH 7.4 by a 10 mM sodium phosphate buffer and were saturated with pyrene (2–3 μM). The stock solutions were prepared using all of the surfactants and **1**, using the buffered pyrene solution. A 10.0 mM quartz cuvette was used to record the emission spectra on an Edinburgh Instruments FLS-980 spectrometer (Edinburgh Instruments, Livingston, UK). The samples were excited at 337 nm and an emission spectrum was recorded from 350 to 410 nm. All of the fluorescence measurements were performed at ambient temperature.

The NMR spectra were recorded on a Bruker Avance II$^+$ 600 (600.01 MHz for ^1H, 242.89 MHz for ^{31}P) spectrometer (Bruker, Rheinstetten, Germany), equipped with a 5 mm direct detection dual broadband probe, with a gradient coil delivering maximum gradient strength of 53 G cm^{-1}. All of the experiments were performed at a temperature of 293 K. The DOSY spectra were measured using a convection compensating double-stimulated echo-based pulse sequence (dstegp3s), with monopolar square shaped gradient pulses. The spectra were acquired with 64k time domain data points in a t2 dimension, with 32 gradient strength increments, a diffusion delay of 100 ms, a gradient pulse length of 4 ms, 16 transients for each gradient step, and a relaxation delay of 2 s. The gradient strength was incremented from 4% to typically 70% of the maximum gradient output (from 1.92 to 33.7 G cm^{-1}). For each sample, the maximum gradient strength was optimized to achieve optimal signal attenuation. The spectra were processed with an exponential window function (line broadening factor 0.5), 64k data points in F2, and 258 data points in the diffusion dimension. The evaluation of the diffusion coefficients was performed by fitting the diffusion profile (the normalized signal intensity as a function of the gradient strength G) at the chemical shift of selected signals in the DOSY spectrum with an exponential function using the variant of the Stejskal–Tanner equation adapted to the particular pulse sequence used.

4. Conclusions

In this work, we explored the effect of the Keggin polyoxometalate $[Zr(\alpha\text{-}PW_{11}O_{39})_2]^{10-}$ on the formation of surfactant-based micelles. Our experiments using fluorescent spectroscopy showed that

the CMCs of the anionic SDS and the neutral TX-100 are unaffected by **1**. DOSY NMR spectroscopy has further revealed that the anionic SDS does not bind with **1** but with the dissolved counter-cations. The neutral TX-100 is not affected by **1** or by the dissolved counteractions.

The CMCs of both CHAPS and Zw3-12 are significantly reduced under the influence of **1**. ^{1}H and ^{31}P DOSY NMR spectroscopy indicated that both CHAPS and Zw3-12 interact with **1** and its counter ion, $Et_2NH_2^+$. However, on the basis of ^{31}P NMR and fluorescence spectroscopy, it was shown that the encapsulated POM species preserves its dimeric structure in the CHAPS/**1** complex, while the interaction with Zw3-12 resulted in structural transformations of the POM with the formation of monomeric Keggin type species with a lower overall negative charge.

The overall work exhibits interesting aspects and offers an important contribution to the interactions of POMs and surfactants in aqueous media. The overall study is also useful for future theoretical studies focusing on molecular dynamics, which could provide further insights into the packing of individual POMs within the forming micelles [56].

Supplementary Materials: The following is available online at http://www.mdpi.com/2304-6740/6/4/112/s1, Figure S1: The emission spectra of (a) saturated aqueous pyrene solution (2–3 μM) buffered at pH 7.4 by a 10 mM sodium phosphate solution, (b) The normalized emission of a saturated pyrene solution (2–3 μM) buffered at pH 7.4 by a 10 mM sodium pohosphate solutions in the presence of increasing concentrations of Zw3-12. Figure S2: ^{1}H DOSY spectra of (a) CHAPS/**1** mixture, (b) CHAPS/Et_2NH_2Cl mixture, (c) CHAPS. Figure S3: CHAPS/**1**—^{31}P DOSY. Figure S4: ^{1}H DOSY spectra of (a) Zw3-12/**1** mixture, (b) Zw3-12/Et_2NH_2Cl mixture, (c) Zw3-12. Figure S5: Zw3-12/**1** mixture—^{31}P DOSY. Figure S6: ^{1}H DOSY spectra of (a) SDS/**1** mixture, (b) SDS/Et_2NH_2Cl mixture, (c) SDS. Figure S7: SDS/**1** mixture—^{31}P DOSY. Figure S8: ^{1}H DOSY spectra of (a) TX100/**1** mixture, (b) TX100/Et_2NH_2Cl mixture, (c) TX100. Figure S9: TX100/**1** mixture—^{31}P DOSY. Figure S10: ^{1}H DOSY Et_2NH_2Cl. Figure S11: ^{1}H DOSY of **1**. Figure S12: ^{31}P DOSY of **1**.

Author Contributions: T.Q. and P.S. acquired and analyzed the fluorescence and NMR spectra respectively. The manuscript was written by T.Q., with valuable contributions and corrections by P.S., A.K., and T.P.-V.

Funding: T.Q. thanks Science Foundation Flanders (FWO) for FWO-SB Q7 doctoral fellowship and A.K. thanks Science Foundation Flanders (FWO) for postdoctoral fellowship (166497/12Y9218N). T.P.-V. thanks Science Foundation Flanders (FWO) and KU Leuven for the funding.

Acknowledgments: K.U. Leuven and the Bulgarian Academy of Sciences are kindly thanked for research support.

Conflicts of Interest: The authors declare no conflict of interest.

References

1. Pope, M.T. *Heteropoly and Isopoly Oxometalates*; Springer: Berlin/Heidelberg, Germany, 1983.
2. Kozhevnikov, I. Sustainable heterogeneous acid catalysis by heteropoly acids. In *Green Chemistry—Green Catalysis: Heterogeneous Catalysis*; Anastas, P.T., Crabtree, R.H., Eds.; Wiley-VCH: New York, NY, USA, 2009; Volume 2, pp. 153–174.
3. Wang, S.S.; Yang, G. Recent advances in polyoxometalate-catalyzed reactions. *Chem. Rev.* **2015**, *115*, 4893–4962. [CrossRef] [PubMed]
4. Clemente-Juan, J.M.; Coronado, E.; Gaita-Arino, A. Magnetic polyoxometalates: From molecular magnetism to molecular spintronics and quantum computing. *Chem. Soc. Rev.* **2012**, *41*, 7464–7478. [CrossRef] [PubMed]
5. Müller, A.; Peters, F.; Pope, M.T.; Gatteschi, D. Polyoxometalates: Very large clusters—Nanoscale magnets. *Chem. Rev.* **1998**, *98*, 239–271. [CrossRef] [PubMed]
6. Absillis, G.; Cartuyvels, E.; Van Deun, R.; Parac-Vogt, T.N. Hydrolytic cleavage of an RNA-model phosphodiester catalyzed by a highly negatively charged polyoxomolybdate $[Mo_7O_{24}]^{6-}$ cluster. *J. Am. Chem. Soc.* **2008**, *130*, 17400–17408. [CrossRef] [PubMed]
7. Ly, H.G.; Absillis, G.; Janssens, R.; Proost, P.; Parac-Vogt, T.N. Highly amino acid selective hydrolysis of myoglobin at aspartate residues as promoted by zirconium(IV)-substituted polyoxometalates. *Angew. Chem. Int. Ed.* **2015**, *54*, 7391–7394. [CrossRef] [PubMed]
8. Luong, T.K.N.; Govaerts, I.; Robben, J.; Shestakova, P.; Parac-Vogt, T.N. Polyoxometalates as artificial nucleases: Hydrolytic cleavage of DNA promoted by a highly negatively charged Zr^{IV}-substituted Keggin polyanion. *Chem. Commun.* **2017**, *53*, 617–620. [CrossRef] [PubMed]

9. Van Rompuy, L.; Parac-Vogt, T.N. Polyoxometalates as sialidase mimics: Selective and non-destructive removal of sialic acid from a glycoprotein promoted by phosphotungstic acids. *Chem. Commun.* **2017**, *53*, 10600–10603. [CrossRef] [PubMed]
10. Sap, A.; Vandebroek, L.; Goovaerts, V.; Martens, E.; Proost, P.; Parac-Vogt, T.N. Highly Selective and Tunable Protein Hydrolysis by a Polyoxometalate Complex in Surfactant Solutions: A Step toward the Development of Artificial Metalloproteases for Membrane Proteins. *ACS Omega* **2017**, *2*, 2026–2033. [CrossRef] [PubMed]
11. Sap, A.; van Tichelen, L.; Mortier, A.; Proost, P.; Parac-Vogt, T.N. Tuning the Selectivity and Reactivity of Metal-Substituted Polyoxometalates as Artificial Proteases by Varying the Nature of the Embedded Lewis Acid Metal Ion. *Eur. J. Inorg. Chem.* **2016**, *32*, 5098–5105. [CrossRef]
12. Sap, A.; De Zitter, E.; van Meervelt, L.; Parac-Vogt, T.N. Structural Characterization of the Complex between Hen Egg-White Lysozyme and Zr^{IV}-Substituted Keggin Polyoxometalate as Artificial Protease. *Chem. Eur. J.* **2015**, *21*, 11692–11695. [CrossRef] [PubMed]
13. Quanten, T.; de Maeyer, T.; Shestakova, P.; Parac-Vogt, T.N. Selectivity and reactivity of Zr^{IV} and Ce^{IV} substituted Keggin type polyoxometalates towards cytochrome c in surfactants solutions. *Front. Chem.* **2018**, *6*, 372. [CrossRef] [PubMed]
14. Quanten, T.; Shestakova, P.; Van Den Bulck, D.; Kirschhock, C.; Parac-Vogt, T.N. Interaction Study and Reactivity of Zr^{IV}-Substituted Wells–Dawson Polyoxometalate towards Hydrolysis of Peptide Bonds in Surfactant Solutions. *Chem. Eur. J.* **2016**, *22*, 3775–3784. [CrossRef] [PubMed]
15. Tanford, C. The hydrophobic effect and the organization of living matter. *Science* **1978**, *200*, 1012–1018. [CrossRef] [PubMed]
16. Kurth, D.G.; Lehmann, P.; Volkmer, D.; Cölfen, H.; Koop, M.J.; Müller, A.; Du Chesne, A. Surfactant-Encapsulated Clusters (SECs): $(DODA)_{20}(NH_4)[H_3Mo_{57}V_6(NO)_6O_{183}(H_2O)_{18}]$, a Case Study. *Chem. Eur. J.* **2000**, *6*, 385–393. [CrossRef]
17. Kurth, D.G.; Lehmann, P.; Volkmer, D.; Müller, A.; Schwahn, D.J. Biologically inspired polyoxometalate–surfactant composite materials. Investigations on the structures of discrete, surfactant-encapsulated clusters, monolayers, and Langmuir–Blodgett films of $(DODA)_{40}(NH_4)_2[(H_2O)_n \subset Mo_{132}O_{372}(CH_3CO_2)_{30}(H_2O)_{72}]$. *Chem. Soc. Dalton Trans.* **2000**, 3989–3998. [CrossRef]
18. Bu, W.; Fan, H.; Wu, L.; Hou, X.; Hu, C.; Zhang, G.; Zhang, X. Surfactant-Encapsulated Polyoxoanion: Structural Characterization of Its Langmuir Films and Langmuir−Blodgett Films. *Langmuir* **2002**, *18*, 6398–6403. [CrossRef]
19. Zhang, B.; Yin, P.; Haso, F.; Hu, L.; Liu, T. Soft Matter Approaches for Enhancing the Catalytic Capabilities of Polyoxometalate Clusters. *J. Clust. Sci.* **2014**, *25*, 695–710. [CrossRef]
20. Nisar, A.; Wang, X. Surfactant-encapsulated polyoxometalate building blocks: Controlled assembly and their catalytic properties. *Dalton Trans.* **2012**, *41*, 9832–9845. [CrossRef] [PubMed]
21. Van Lokeren, L.; Cartuyvels, E.; Absillis, G.; Willem, R.; Parac-Vogt, T.N. Phosphoesterase activity of polyoxomolybdates: Diffusion ordered NMR spectroscopy as a tool for obtaining insights into the reactivity of polyoxometalate clusters. *Chem. Commun.* **2008**, *0*, 2774–2776. [CrossRef] [PubMed]
22. Shestakova, P.; Absillis, G.; Martinez, F.J.; De Proft, F.; Willem, R.; Parac-Vogt, T.N. Integrating ^{31}P DOSY NMR Spectroscopy and Molecular Mechanics as a Powerful Tool for Unraveling the Chemical Structures of Polyoxomolybdate-Based Amphiphilic Nanohybrids in Aqueous Solution. *Chem. Eur. J.* **2014**, *20*, 5258–5270. [CrossRef] [PubMed]
23. Luong, T.K.N.; Shestakova, P.; Absillis, G.; Parac-Vogt, T.N. Detailed Mechanism of Phosphoanhydride Bond Hydrolysis Promoted by a Binuclear Zr^{IV}-Substituted Keggin Polyoxometalate Elucidated by a Combination of 31P, 31P DOSY, and 31P EXSY NMR Spectroscopy. *Inorg. Chem.* **2016**, *55*, 4864–4873. [CrossRef] [PubMed]
24. Kalyanasundaram, K.; Thomas, J.K. Environmental effects on vibronic band intensities in pyrene monomer fluorescence and their application in studies of micellar systems. *J. Am. Chem. Soc.* **1977**, *99*, 2039–2044. [CrossRef]
25. Kalyanasundaram, K. Chapter 1—Introduction. In *Photochemistry in Microheterogeneous Systems*; Kalyanasundaram, K., Ed.; Academic Press Inc.: Orlando, FL, USA, 1987; pp. 36–91. ISBN 978-0-12-394995-0.
26. Liu, X.-F.; Dong, L.-L.; Fang, Y. Synthesis and Self-Aggregation of a Hydroxyl-Functionalized Imidazolium-Based Ionic Liquid Surfactant in Aqueous Solution. *J. Surf. Deterg.* **2010**, *14*, 203–210. [CrossRef]

27. Quagliotto, P.; Barbero, N.; Barolo, C.; Costabello, K.; Marchese, L.; Coluccia, S.; Kalyanasundaram, K.; Viscardi, G. Characterization of monomeric and gemini cationic amphiphilic molecules by fluorescence intensity and anisotropy. *Dyes Pigments* **2009**, *82*, 124–129. [CrossRef]
28. Matsuoka, K.; Suzuki, M.; Honda, C.; Endo, K.; Moroi, Y. Micellization of conjugated chenodeoxy- and ursodeoxycholates and solubilization of cholesterol into their micelles: Comparison with other four conjugated bile salts species. *Chem. Phys. Lipids* **2006**, *139*, 1–10. [CrossRef] [PubMed]
29. Howell, S.C.; Mittal, R.; Huang, L.; Travis, B.; Breyer, R.M.; Sanders, C.R. CHOBIMALT: A Cholesterol-Based Detergent. *Biochemistry* **2010**, *49*, 9572–9583. [CrossRef] [PubMed]
30. Hierrezuelo, J.M.; Aguiar, J.; Carnero Ruiz, C. Synergism in mixtures of zwitterionic and ionic surfactants. *J. Colloid Interface Sci.* **2006**, *294*, 449–457. [CrossRef] [PubMed]
31. Sabate, R.; Estelrich, J. Evidence of the Existence of Micelles in the Fibrillogenesis of β-Amyloid Peptide. *J. Phys. Chem. B* **2005**, *109*, 11027–11032. [CrossRef] [PubMed]
32. Gaspar, V.M.; Goncalves, C.; de Melo-Diogo, D.; Costa, E.C.; Queiroz, J.A.; Pichon, C.; Sousa, F.; Correia, I.J. Poly(2-ethyl-2-oxazoline)-PLA-*g*-PEI amphiphilic triblock micelles for co-delivery of minicircle DNA and chemotherapeutics. *J. Control. Release* **2014**, *189*, 90–104. [CrossRef] [PubMed]
33. Mok, M.M.; Thiagarajan, R.; Flores, M.; Morse, D.C.; Lodge, T.P. Apparent Critical Micelle Concentrations in Block Copolymer/Ionic Liquid Solutions: Remarkably Weak Dependence on Solvophobic Block Molecular Weight. *Macromolecules* **2012**, *45*, 4818–4829. [CrossRef]
34. Piogé, S.; Fontaine, L.; Gaillard, C.; Nicol, E.; Pascual, S. Self-Assembling Properties of Well-Defined Poly(ethylene oxide)-*b*-poly(ethyl acrylate) Diblock Copolymers. *Macromolecules* **2009**, *42*, 4262–4272. [CrossRef]
35. Feitosa, E.; Brown, W.; Vasilescu, M.; Swanson-Vethamuthu, M. Effect of Temperature on the Interaction between the Nonionic Surfactant $C_{12}E_5$ and Poly(ethylene oxide) Investigated by Dynamic Light Scattering and Fluorescence Methods. *Macromolecules* **1996**, *29*, 6837–6846. [CrossRef]
36. Evertsson, H.; Nilsson, S.; Holmberg, C.; Sundelöf, L.-O. Temperature Effects on the Interactions between EHEC and SDS in Dilute Aqueous Solutions. Steady-State Fluorescence Quenching and Equilibrium Dialysis Investigations. *Langmuir* **1996**, *12*, 5781–5789. [CrossRef]
37. Aguiar, J.; Carpena, P.; Molina-Bolívar, J.A.; Carnero Ruiz, C. On the determination of the critical micelle concentration by the pyrene 1:3 ratio method. *J. Colloid Interface Sci.* **2003**, *258*, 116–122. [CrossRef]
38. Anthony, O.; Zana, R. Fluorescence Investigation of the Binding of Pyrene to Hydrophobic Microdomains in Aqueous Solutions of Polysoaps. *Macromolecules* **1994**, *27*, 3885–3891. [CrossRef]
39. Regev, O.; Zana, R. Aggregation Behavior of Tyloxapol, a Nonionic Surfactant Oligomer, in Aqueous Solution. *J. Colloid Interface Sci.* **1999**, *210*, 8–17. [CrossRef] [PubMed]
40. Tiller, G.E.; Mueller, T.J.; Dockter, M.E.; Struve, W.G. Hydrogenation of Triton X-100 eliminates its fluorescence and ultraviolet light absorption while preserving its detergent properties. *Anal. Biochem.* **1984**, *141*, 262–266. [CrossRef]
41. Brown, W.; Rymden, R.; Van Stam, J.; Almgren, M.; Svensk, G. Static and dynamic properties of nonionic amphiphile micelles: Triton X-100 in aqueous solution. *J. Phys. Chem.* **1989**, *93*, 2512–2519. [CrossRef]
42. Denkova, P.S.; Lokeren, L.V.; Verbruggen, I.; Willem, R. Self-Aggregation and Supramolecular Structure Investigations of Triton X-100 and SDP2S by NOESY and Diffusion Ordered NMR Spectroscopy. *J. Phys. Chem. B* **2008**, *112*, 10935–10941. [CrossRef] [PubMed]
43. Chattopadhyay, A.; London, E. Fluorimetric determination of critical micelle concentration avoiding interference from detergent charge. *Anal. Biochem.* **1984**, *139*, 408–412. [CrossRef]
44. Giacomelli, C.E.; Vermeer, A.W.P.; Norde, W. Micellization and Adsorption Characteristics of CHAPS. *Langmuir* **2000**, *16*, 4853–4858. [CrossRef]
45. Qin, X.; Liu, M.; Yang, D.; Zhang, X. Concentration-Dependent Aggregation of CHAPS Investigated by NMR Spectroscopy. *J. Phys. Chem. B* **2010**, *114*, 3863–3868. [CrossRef] [PubMed]
46. Stark, R.E.; Leff, P.D.; Milheim, S.G.; Kropf, A. Physical studies of CHAPS, a new detergent for the study of visual pigments. *J. Phys. Chem.* **1984**, *88*, 6063–6067. [CrossRef]
47. Schuerholz, T.; Kehne, J.; Gieselmann, A.; Neumann, E. Functional reconstitution of the nicotinic acetylcholine receptor by CHAPS dialysis depends on the concentrations of salt, lipid, and protein. *Biochemistry* **2002**, *31*, 5067–5077. [CrossRef]

48. Hjelmeland, L.M.; Nebert, D.W.; Osborne, J.C. Sulfobetaine derivatives of bile acids: Nondenaturing surfactants for membrane biochemistry. *Anal. Biochem.* **1983**, *130*, 72–82. [CrossRef]
49. Vulliezlenormand, B.; Eisele, J.L. Determination of Detergent Critical Micellar Concentration by Solubilization of a Colored Dye. *Anal. Biochem.* **1993**, *208*, 241–243. [CrossRef]
50. Neugebauer, J.M. Detergents: An overview. *Meth. Enzymology* **1990**, *182*, 239–253.
51. Samsonoff, C.; Daily, J.; Almog, R.; Berns, D.S. The use of Coomassie brilliant blue for critical micelle concentration determination of detergents. *J. Colloid Interface Sci.* **1986**, *109*, 325–329. [CrossRef]
52. Johnson, C.S., Jr. Diffusion ordered nuclear magnetic resonance spectroscopy: principles and applications. *Prog. Nucl. Magn. Reson. Spectrosc.* **1999**, *34*, 203–256. [CrossRef]
53. Sokolov, M.N.; Chubarova, E.V.; Peresypkina, E.V.; Virovets, A.V.; Fedin, V.P. Complexes of Zr^{IV} and Hf^{IV} with monolacunary Keggin- and Dawson-type anions. *Russ. Chem. Bull.* **2007**, *56*, 220–224. [CrossRef]
54. Kato, C.N.; Shinohara, A.; Hayashi, K.; Nomiya, K. Syntheses and X-ray Crystal Structures of Zirconium(IV) and Hafnium(IV) Complexes Containing Monovacant Wells–Dawson and Keggin Polyoxotungstates. *Inorg. Chem.* **2006**, *45*, 8108–8119. [CrossRef] [PubMed]
55. Kondinski, A.; Parac-Vogt, T.N. Keggin Structure, Quō Vādis? *Front. Chem.* **2018**, *6*, 364. [CrossRef] [PubMed]
56. Solé-Daura, A.; Goovaerts, V.; Stroobants, K.; Absillis, G.; Jiménez-Lozano, P.; Poblet, J.M.; Hirst, J.D.; Parac-Vogt, T.N.; Carbó, J.J. Probing Polyoxometalate–Protein Interactions Using Molecular Dynamics Simulations. *Chem. Eur. J.* **2016**, *22*, 15280–15289. [CrossRef] [PubMed]